


GaSb Swept-Wavelength Lasers for Biomedical Sensing Applications

Augustinas Vizbaras , Ieva Šimonytė, Serge Droz, Nicolas Torcheboeuf, Arūnas Miasojedovas, Augustinas Trinkūnas, Tadas Bučiūnas, Žilvinas Dambrauskas, Antanas Gulbinas, Dmitri L. Boiko, and Kristijonas Vizbaras

(Invited Paper)

Abstract—Infrared spectral range between 1.7 and 2.5 μm is of particular interest for biomedical sensing applications due to the presence of first overtone C–H stretch and a combination of stretch and bending vibrations of C–H, N–H, and O–H bonds. These vibrations are molecule specific and can be used to selectively sense important biomolecules such as glucose, lactate, urea, ammonia, serum albumin, etc. In this paper, we review recent developments of swept-wavelength lasers based on GaSb type-I gain-chip technology, their key performance parameters for spectroscopy applications and provide experimental data on spectroscopic sensing of the key biomolecules both in synthetic solutions as well as whole blood.

Index Terms—Swept-wavelength laser, tunable laser, spectroscopic sensing, gallium antimonide, glucose sensor, biosensor, linewidth.

I. INTRODUCTION

SPECTROSCOPIC laser sensing is an attractive sensing technique not only because of the sensitivity and specificity but also due to the ability to perform sensing in a large dynamic concentration range as well as offer multi-component sensing capability [1]. Semiconductor lasers are key components in building spectroscopic sensing instruments due to their nature of technology-compactness, scalability, efficiency and potential for low-cost offering the best Size-Weight and Power-Cost (SWaP-C) properties among the types of different lasers.

Manuscript received January 29, 2019; revised April 16, 2019; accepted May 1, 2019. Date of publication May 10, 2019; date of current version June 24, 2019. This work was supported by EUROSTARS-2 E10051 Project SWIRsense. (Corresponding author: Augustinas Vizbaras.)

A. Vizbaras, I. Šimonytė, A. Miasojedovas, A. Trinkūnas, T. Bučiūnas, and K. Vizbaras are with the Brolis Semiconductors UAB LT-14259 Vilnius, Lithuania (e-mail: augustinas.vizbaras@brolis-semicon.com; ieva.simonyte@brolis-semicon.com; arunas.miasojedovas@brolis-semicon.com; augustinas.trinkunas@brolis-semicon.com; tadas.buciuнас@brolis-semicon.com; kristijonas.vizbaras@brolis-semicon.com).

S. Droz, N. Torcheboeuf, and D. L. Boiko are with the Centre Suisse d'Electronique et de Microtechnique SA (CSEM), Neuchâtel CH-2002 Switzerland (e-mail: serge.droz@csem.ch; Nicolas.TORCHEBOEUF@csem.ch; dmitri.boiko@csem.ch).

Ž. Dambrauskas and A. Gulbinas are with the Institute for Digestive Research, Medical Academy, Lithuanian University of Health Sciences, LT-50161, Kaunas Lithuania (e-mail: zilvinas.dambrauskas@ismuni.lt; antanas.gulbinas@ismuni.lt).

Color versions of one or more of the figures in this paper are available online at <http://ieeexplore.ieee.org>.

Digital Object Identifier 10.1109/JSTQE.2019.2915967

For spectroscopic sensing, the ability to emit narrow linewidth laser emission at the object-specific wavelength and the ability to tune the emission wavelength is most important. Wavelength selection is typically achieved by realizing distributed feedback gratings (DFB) within the laser cavity, and wavelength tuning is performed by simply changing the current. In this way, the laser can tune several nm, which is in most cases sufficient for sensing small gas molecules such as CO, CO₂, N₂O, CH₃, SO₂ etc [2], [3]. However, in cases where sensing of multiple molecules is of interest or where the specific ro-vibrational absorption spectra are broadened due to collisions (for instance in a liquid phase) or in case of long molecules such as polymers or proteins, a much wider tuning band is required [4], [5]. In such application cases the tuning bandwidth of a single DFB laser is not sufficient. Therefore different approaches should be considered, such as DFB arrays [6], or complex monolithic widely tunable lasers based on sampled gratings [7], [8] or external cavity diode lasers (ECDLs) [5]–[9]. Both DFB arrays and widely tunable monolithic lasers are well matured for telecom wavelengths but the related fabrication techniques are difficult to transfer to other spectral bands as they require complex fabrication and processing technology steps such as E-beam lithography, multiple epitaxial growth steps etc. Therefore, the broadband semiconductor laser-based spectroscopy is mostly performed using ECDLs, where a semiconductor gain-chip with very low reflectivity facet coating acts as a broadband gain material while the wavelength filtering and tuning is performed by an external diffraction grating. This technology enables a coverage of wide spectral bands in the visible, mid-IR or long-wave infrared ranges with the infrared range coverage based primarily on the quantum cascade laser (QCL) technology [5]–[9]. Most of the mentioned approaches, are bulky, expensive and rather delicate to operate. It is worth to mention the efforts on transferring the ECDL architecture to the microelectromechanical systems (MEMS) technology implementation [10], but so far these efforts were mainly limited to near-infrared and telecom spectral bands.

In this work we review our recent developments of widely tunable laser sources for largely unexplored spectral region of 1.7–2.5 μm in between the near-IR and mid-IR bands. This region offers an access to the first overtone of C–H stretch and a combination of stretch and bending vibrations of C–H, O–H,

N-H bonds. It offers more than an order of magnitude better sensitivity vs. the telecom spectral band due to a higher molar absorptivity of the most important biomolecules such as glucose, lactate, urea, serum albumin, creatinine and others [11]. Probably one of the reasons why this spectral band has been overlooked was the lack of efficient semiconductor light sources in this range. Despite the efforts put to realize such tunable lasers [12], [13], their performances remained quite limited. Our work is mostly based on the last decade's GaSb type-I strained QW technology developments. We demonstrate that this technology is matured and offers an excellent choice as optical gain material for the beyond-telecom spectral band [14]–[16] to realize compact swept-wavelength lasers using MEMS technology [17] or ECDLs using hybrid GaSb/Si photonic integrated circuits technology [18], [19]. In this paper, we review swept wavelength laser (SWL) technology in terms of the performance, linewidth, spectral purity, wavelength tuning continuity and tuning speed. We provide application examples for spectroscopic sensing of critical biomolecules including a powerful technology demonstrator of glucose sensing in whole blood.

II. GaSb GAIN-CHIP TECHNOLOGY

A. Epitaxial Growth

The gain-chip device wafers were epitaxially grown on 3-inch Te doped $n+$ GaSb substrates using an industrial solid-source multi-wafer molecular beam epitaxy machine, equipped with Al, Ga, In, As, Sb as elemental source materials and Si, GaTe and Be as dopant sources. The device layer sequence was started with a 50 nm n -doped GaSb buffer followed by a 60 nm thick $\text{Al}_x\text{Ga}_{1-x}\text{As}_y\text{Sb}_{1-y}$ linearly graded layer, nominally doped at $1 \times 10^{18} \text{cm}^{-3}$ density and compositionally graded from 0 to 50% on Al content and As concentration adjusted so as to maintain the lattice matching to the substrate. The grading was followed by a 2.2 μm thick lower $\text{Al}_{0.5}\text{Ga}_{0.5}\text{As}_{0.04}\text{Sb}_{0.96}$ cladding, in which first 1500 nm were nominally doped to $3 \times 10^{17} \text{cm}^{-3}$ and the following 700 nm were doped to $7 \times 10^{16} \text{cm}^{-3}$ in order to reduce the free-carrier induced losses of the optical mode. The cladding layer was followed by an undoped $\text{Al}_{0.25}\text{Ga}_{0.75}\text{As}_{0.02}\text{Sb}_{0.98}$ waveguide and a barrier layer, in which two compressively strained quantum wells (QWs) were embedded. QW emission wavelength was tuned by changing the alloy composition in the quantum well. Thus for 1.7 μm wavelength, AlGaInSb QWs were used in the active region. For 1.9 and 2.1 μm emission wavelengths, GaInSb QW material was used. For longer wavelengths, quaternary GaInAsSb QWs were used. QW and waveguide thicknesses were adjusted for a 1% transverse vertical optical confinement factor per QW. For the optical mode symmetry, both waveguide layers on the n and p sides were left nominally undoped. The p – side waveguide was followed by 2.2 μm thick $\text{Al}_{0.5}\text{Ga}_{0.5}\text{As}_{0.04}\text{Sb}_{0.96}$ cladding doped with Be. The first 700 nm of the layer were doped at $1 \times 10^{17} \text{cm}^{-3}$, followed by a 500 nm thick slice doped to $1 \times 10^{18} \text{cm}^{-3}$, while the last 1000 nm of the cladding were doped to $5 \times 10^{18} \text{cm}^{-3}$. Cladding was followed by 60 nm $p+$ $\text{Al}_x\text{Ga}_{1-x}\text{As}_y\text{Sb}_{1-y}$ linear grading and topped with 200 nm of a heavily Be-doped ($1 \times 10^{19} \text{cm}^{-3}$) GaSb p -contact layer.

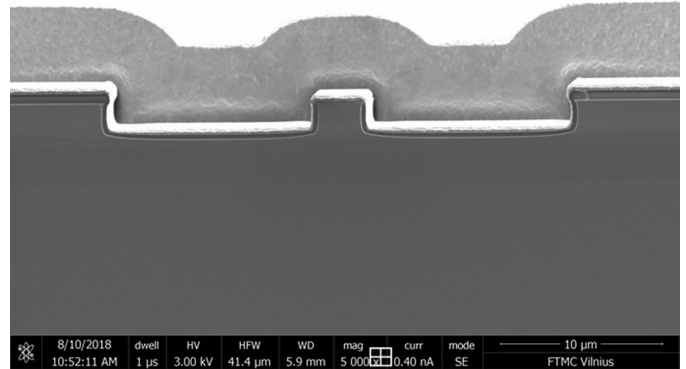


Fig. 1. SEM image of the output facet of the processed GaSb-based gain-chip.

B. Gain-Chip Fabrication

The grown wafers were processed as quasi-index guided single-angled facet (SAF) gain-chip devices. For a single spatial mode output, the 4 μm -wide and $\sim 1.5 \mu\text{m}$ -deep ridge waveguides were defined by UV photolithography and Cl-based ICP-RIE etching, followed by sputtering of a $\sim 330 \text{nm}$ thick SiO_2 insulation layer. A contact window on the top of the ridge was defined by lithography and opened by means of CF_4/O_2 based ICP-RIE dry etching step. E-beam evaporated Ti/Pt/Au was used as a p -ohmic contact followed by a $\sim 2 \mu\text{m}$ thick Au plated heatsink. The wafers were then thinned down to $\sim 120 \mu\text{m}$ to facilitate cleaving. As the last step, the back side Ti/Pt/Au contact was evaporated. The wafers were cleaved into bars of 1 mm and 0.7 mm cavity length and the bar facets were coated. The output facet was then anti-reflection coated to have the reflectivity $< 0.1\%$ and the back facet got a high reflectivity coating with the reflectivity $> 95\%$. Each bar contained 18 angled gain-chips and 2 straight ridge Fabry-Perot (FP) laser chips used as a reference for facet reflectivity measurements and basic laser parameters extraction in order to compare and evaluate the gain-chip performance in external cavity configuration. Fig. 1 shows scanning electron microscope image of the processed gain-chip.

C. Gain-Chip Performance Results

Normalized amplified spontaneous emission (ASE) spectra of five different GaSb gain-chips covering the entire 1.7–2.5 μm spectral range of interest is shown in Fig. 2. Here, the spectrum of the gain-chip emitting around 1.9 μm is affected by the absorption of water vapor in the atmosphere during the spectral acquisition with Fourier-Transform-Infrared (FTIR) spectrometer (Thermo Fisher Nicolet 6700). It can be seen that the ASE spectra are broad with typical FWHM $> 50 \text{nm}$. Moreover, some of the chips clearly exhibit the band filling effect and emission from the higher excited state of the quantum well. This is a known feature of highly strained GaInAsSb QW, which yields a low effective mass of the heavy holes as well as weak electron-phonon interaction. In case of swept-wavelength laser application, this feature is particularly useful as it extends the optical gain bandwidth, yielding extremely broad laser tuning ranges.

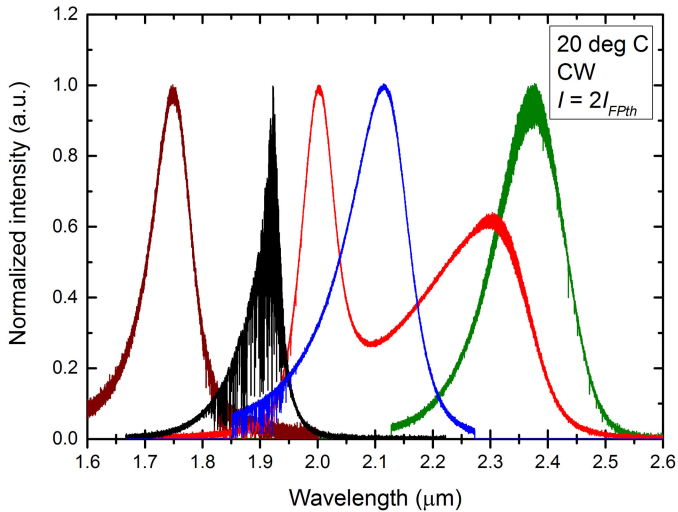


Fig. 2. Normalized ASE emission spectra of five different GaSb gain-chips. Heatsink temperature was stabilized at 20 deg C, drive mode – continuous wave. The drive current was chosen to be twice the threshold value of the reference FP laser within the same wafer. Reproduced from [17].

More specific details on the exact epitaxial structure of the gain-chips can be found in [17]. In free-running mode (ASE) these AR coated gain-chips provide CW output powers up to 5 mW, which in most cases is limited by a thermal roll-over and a strong non-radiative recombination such as the Auger process [16] at a high carrier density. Note however that the ASE output power of the gain-chip does not provide a reliable insight about the expected laser output power from the same gain-chip embedded in an external cavity and operating at a clamped carrier density. We observe that the gain-chips emitting <1 mW in ASE mode can provide >50 mW of laser output power in the external cavity configuration.

III. SWEPT-WAVELENGTH LASER

A. External Cavity Swept-Wavelength Laser Configuration

Gain-chip is the key enabling component of the external cavity laser diode where its properties determine such critical performance parameters of the ECDL as tuning bandwidth, linewidth, noise and output power, which essentially define the potential application scenario. In this section we describe the concept of the MEMS based SWL and provide a deep insight into the microscopic parameters, physical properties and characteristics of the gain-chip and laser itself.

Fig. 3 shows the photographic image of the MEMS based ECDL which we used as a test bed. The GaSb-based gain-chip was embedded into an external cavity based on Littman-Metcalf configuration. A commercial off-the-shelf holographic diffraction grating with 600 groves/mm and blaze wavelength of 1200 nm was used in combination with a commercial high NA aspheric lens for beam collimation. The wavelength tuning was achieved by closing the ECDL cavity with electrically driven tilt-tunable Au coated MEMS mirror. It has a mechanical resonance frequency of ~ 200 Hz and the tilt angle dynamic range from

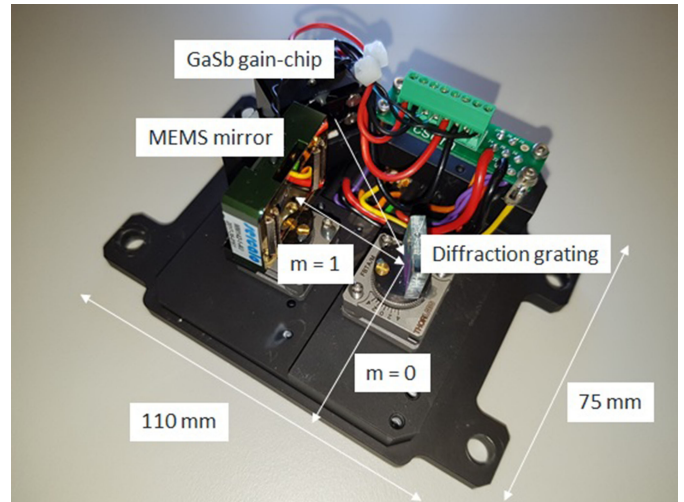


Fig. 3. Top-view of the MEMS based GaSb swept-wavelength laser based on Littman-Metcalf configuration with the main building blocks indicated in the picture.

-5 to $+5$ degrees. We reached a reasonable spectral resolution and performance with the mirror sweep frequencies up to 150 Hz, collecting the spectral curve data at the rate of 300 sweeps/s.

B. Microscopic Parameter Extraction

In order to extract the microscopic parameters of the gain-chip used in our SWLs, we perform Hakki–Paoli measurements of amplified spontaneous emission (ASE) and lasing spectra. We extract the modal gain, spontaneous emission, and the phase-amplitude coupling coefficient α_H [20] for one of the selected gain-chips, with the gain peak close to $2.2 \mu\text{m}$ wavelength. The spectral measurements were performed in the dispersion-free 0th diffraction order output beam of the ECDL using an optical spectrum analyzer (Yokogawa, AQ6375B). For taking the ASE spectra, the 1st order diffraction beam incident on the MEMS cavity mirror was blocked while we continued using the dispersion-free 0th diffraction order of the cavity grating for spectral measurements. The lasing regime with MEMS cavity tuned for specific wavelength allowed us to perform spectral measurement at a carrier density clamped to its threshold value (Fig. 4), while measurements in the ASE regime allowed it to vary (Fig. 5). In both cases, we studied the behavior of the Fabry-Perot fringes on the ASE pedestal modulated due to the residue facet reflectivity of the gain chip. At a clamped carrier density, their red shift with the current is due to thermal effects (Fig. 4, inset), while in the ASE case, the blue shift is due to the interplay between the carrier induced refractive index change and temperature effects (Fig. 5, inset). In addition to the behavior of the net modal gain coefficient with the temperature and pump current, we extracted the phase amplitude coupling coefficient α_H by taking a difference between the two measurements in Figs. 4 and 5 [21]. Note that a strong phase amplitude coupling in semiconductor laser increases the frequency noise and causes the linewidth enhancement by a factor of $1 + \alpha_H^2$.

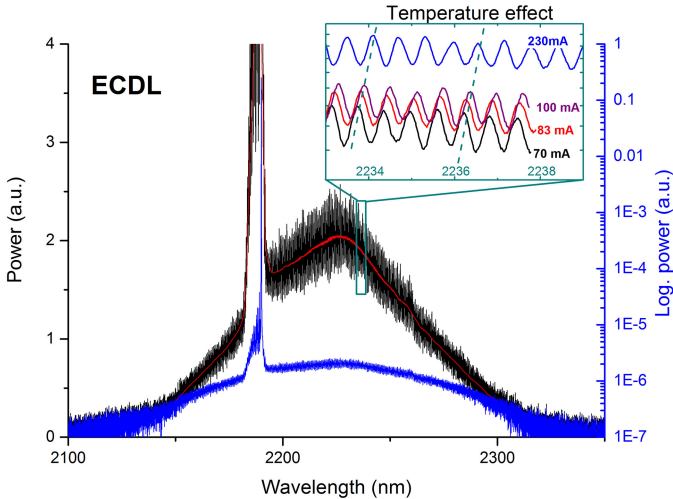


Fig. 4. Lasing spectrum in GaSb ECDL at 230 mA pump current plotted in logarithmic scale (blue curve, right axis) and in a linear scale at the ASE pedestal (black curve, left axis) showing the FP cavity fringes due to chip facet reflections. The red curve is a fringe-averaged ASE from the chip at clamped carrier density. The inset shows a zoom on the fringe shift with the pump current. The red shift with the pump current is a purely temperature effect because the carriers are clamped at threshold density.

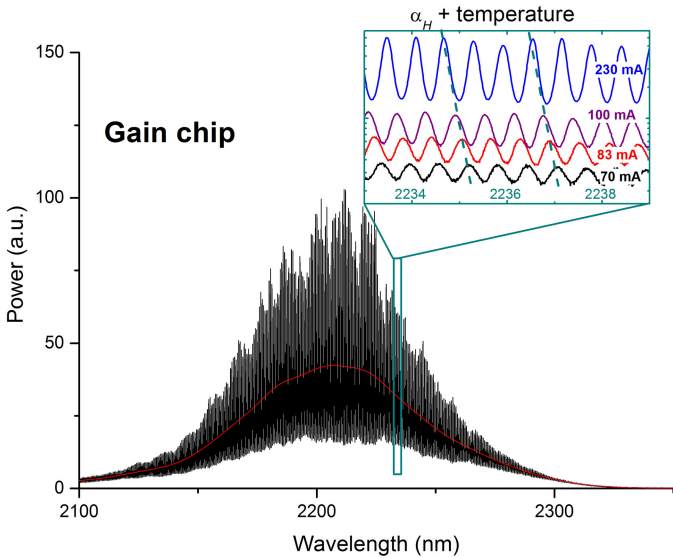


Fig. 5. Spontaneous emission spectrum in GaSb gain chip at 230 mA pump current (black curve, left axis). The red curve is a fringe-averaged ASE from the chip. The inset shows a zoom on the fringe shift with the pump current. The net blue shift with the pump current is due to an interplay between the carrier induced refractive index change and temperature effects.

Using the relationship

$$ASE(\lambda) = -SE(\lambda)/\tilde{G}(\lambda)L_G \quad (1)$$

between, the spectral components of the net modal gain coefficient \tilde{G} in the free-running gain chip times the gain chip length L_G and the resulting amplified spontaneous emission $ASE(\lambda)$, we extracted the spectral profile of an unamplified spontaneous emission $SE(\lambda)$. It defines the spectrum of the noise source in our laser.

Using 0.1% front facet AR coating and 98% rear facet reflectivity values [17], we estimated the cold cavity losses in our

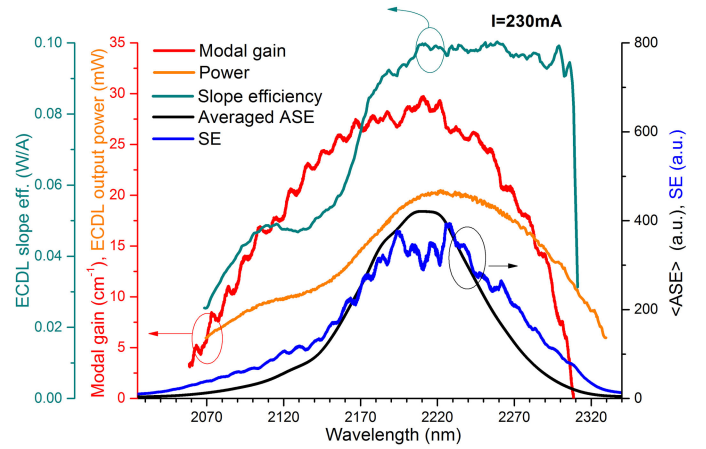


Fig. 6. Modal gain curve, spontaneous emission and fringe-averaged amplified spontaneous emission in free running GaSb chip of 1 mm length as well as the ECDL power and ECDL differential slope efficiency curves for the same chip embedded in the external cavity. All measurements are performed at the pump current of 230 mA.

1 mm long chip to be of 36.6 cm^{-1} . Adding this constant value to the measured net modal gain we obtained the modal gain curve $G(\lambda)$ which is plotted in Fig. 6 (red curve, left axis). In this figure we also plot the FP-fringe-averaged ASE spectrum in comparison with the extracted unamplified SE (black and blue curves, right axis). As expected, the true SE, ASE and the optical gain G curves have slightly different spectral profiles, but all of them are centered nearby 2190 nm wavelength and reveal broad spectral widths. Thus, the optical gain spectrum is of 180 nm FWHM. For comparison, a typical NIR GaAs or InGaAsP QW lasers provide optical gain bandwidth of only 30–50 nm wide. Such a broad gain curve in GaSb type-I QWs renders them highly attractive not only for building widely tunable lasers for various spectroscopy applications [17] but also for realizing ultrafast infrared mode-locked lasers [22].

Figure 6 shows also the resulting output power variation in our GaSb ECDL when the ECDL wavelength is tuned with the MEMS mirror tilt angle. Surprisingly, the spectral profile of the output power curve does not follow the gain curve shape while it reproduces well the steps in the differential slope efficiency curve. Therefore we attribute this shape to the injection efficiency of heavy holes into GaSb quantum wells, which is subjected to the band filling effect and is different for the emission from the ground and excited states of the well [16].

Performing such spectral measurements at different pump currents and gain chip submount temperatures we extract the key optical gain and noise parameters as well as the temperature and current tuning coefficients. These are summarized in Fig. 7 and Table I. In Fig. 7, we plot a dispersion of the transparency current J_{tr} and of the logarithmic modal gain coefficient G_0 [the overall modal gain is $G = G_0 \ln(J/J_{tr})$]. Their values at the center of the gain curve are quoted in Table I. For our ECDL with the cavity length of 7.5 cm and grating efficiency of 9% in the double-pass Littman-Metcalf configuration, the threshold gain is 12.7 cm^{-1} . In Fig. 7 we plot the estimated threshold current dispersion, which agrees well with the experiment.

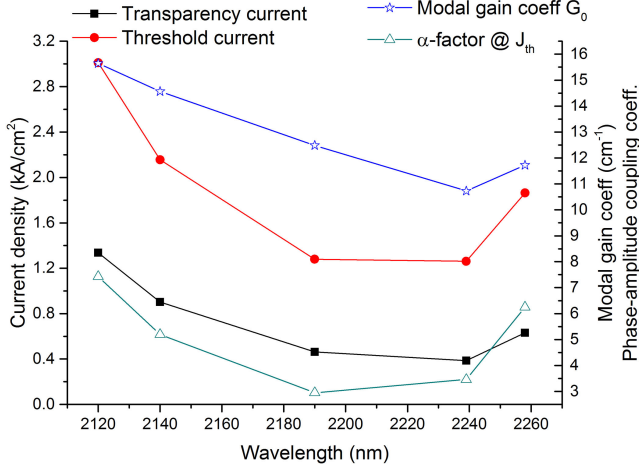


Fig. 7. Dispersion of the transparency and ECDL threshold current densities (left axes) as well as of the logarithmic modal gain coefficient and the phase amplitude coupling factor α_H (right axis).

TABLE I
EXTRACTED PARAMETERS OF GaSb GAIN CHIP

Symbol	Quantity	Conversion from Gaussian and CGS EMU to SI ^a
$d\lambda_0/dT$	Peak gain wavelength temperature coeff	1.17025nm/°C
dn_g/dT	Group index temp. coeff.	0.00266/°C
R_T	Thermal mounting resistance	23.98 K/W
$d\lambda_{FP}/dT$	FP cavity (or DFB) wavelength temperature coeff.	0.064 nm/K
$d\lambda_{FP}/dI$	FP cavity (or DFB) wavelength current coeff.	0.00186 nm/mA
n_g	Group velocity index	4.05 *)
G_0	Logarithmic gain coefficient	12.6 cm ⁻¹ *)
J_r	Transparency current density	0.44 kA/cm ² *)
J_{th}	Threshold current density	1.3 kA/cm ² *)
α_H	Phase amplitude coupling coefficient at threshold	2.95 *) **)

*) Values are specified at the gain maxim 2190 nm. **) at ECDL threshold

In general, the linewidth enhancement factor α_H varies strongly with the wavelength and carrier density [21]. We also observe such strong variation of α_H in our GaAs gain chip. In Fig. 7, we report its spectral behavior for the clamped carrier density at ECDL threshold, accounting for the dispersion of the threshold current. Out of 5 selected emission wavelengths, the lowest linewidth enhancement is at 2190 nm, which is close to the gain maximum.

The extracted microscopic parameters of the GaSb type-I QW gain-chip provides useful information regarding their suitability for precision spectroscopic instruments or can serve as useful input data for modelling other type of tunable lasers in this material system such as DFB, DBR, VCSEL etc.

C. Swept-Wavelength Laser Performance

In this section we discuss the main performance results of the swept-wavelength lasers based on the GaSb gain-chips

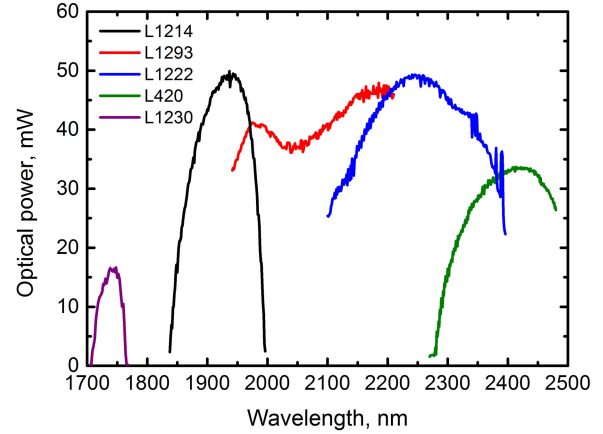


Fig. 8. CW output power vs. wavelength for five GaSb-based SWLs. Heatsink temperature was stabilized at 20 degrees C.

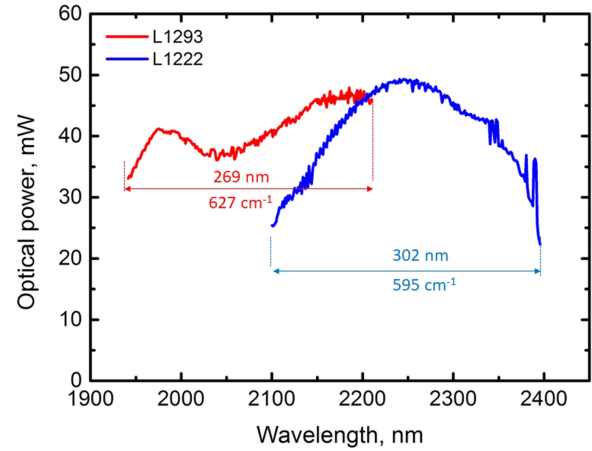


Fig. 9. Wavelength tuning characteristics of two ultra-broad bandwidth MEMS-ECDLs with different wavelength gain-chip designs. Heatsink temperature was kept at 20 degrees C, laser was driven at 770 mA in CW mode.

with a closer look into the tuning behavior offered by the MEMS ECDL. Experimental wavelength tuning characteristics are shown in Fig. 8 for the SWLs based on the gain-chips presented in Fig. 2. It can be seen that MEMS driven GaSb-based SWLs demonstrate excellent tuning characteristics in terms of bandwidth and output power. Except for the SWL, centered at 1.7 μm , all of the lasers demonstrate tuning bandwidths in excess of 400 cm^{-1} while maintaining output power above 10 mW. While these results are already beyond state-of-the-art, in Fig. 9, we report superior experimental data obtained for our latest optimized selected swept-wavelength lasers, centered around 2.1 and 2.25 μm . Here, the tuning bandwidths of 627 cm^{-1} or 77.8 meV and 595 cm^{-1} or 74 meV with output power equal or greater than 20 mW is achieved. To the best of our knowledge this is the largest tuning bandwidth achieved with single GaSb gain-chip, exceeding the recent state-of-the-art by more than 100 cm^{-1} [23]. It clearly demonstrates the potential for spectroscopy applications of the direct type-I quantum well GaSb technology, as a single broadband chip can replace more than 10 separate DFB lasers.

One of the peculiarities of the MEMS based SWL is related to small controllable mode-hops occurring because the MEMS

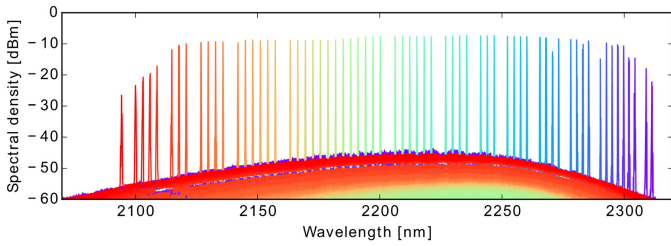


Fig. 10. False-colored superimposed optical spectra at various MEMS mirror tilt angles showing continuous tuning over 220 nm and SMSR of >50 dB .

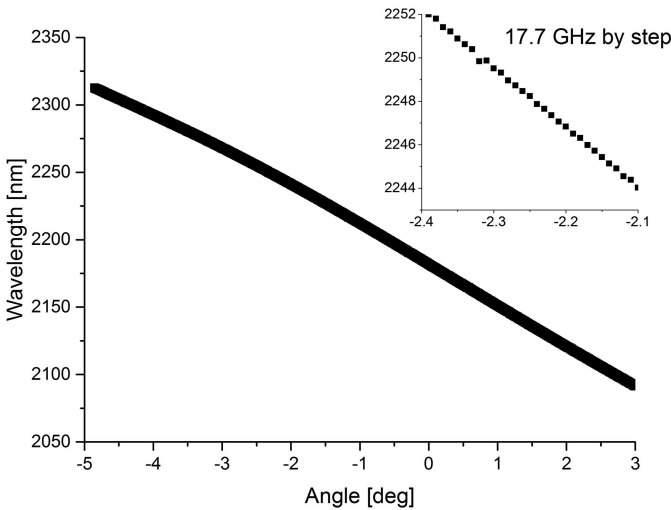


Fig. 11. Lasing wavelength in function of the MEMS mirror angle. The inset shows a zoom revealing individual tuning steps.

mirror cannot be positioned at a “sweet” pivot axis location for mode-hop-free tuning [9]–[24]. As we discuss below, this is not a limitation for a large number of spectroscopic sensing applications, e.g., for applications targeting broad spectral signatures in liquids.

D. Mode-Hopping Characteristics

In our approach, a proven Littman-Metcalf external cavity configuration with the double pass over the grating per cavity roundtrip was selected. However instead of a complex cavity opto-mechanics with dedicated location of the pivoting axis for a retroreflector [24], we close the cavity with a light-weight tunable MEMS mirror and use an extremely well AR treated GaSb gain chip for spectral purity and selectivity.

Fig 10 shows tuning of the lasing spectra at various tilt angles of the MEMS mirror for a selected GaSb based SWL with center wavelength $\sim 2.2 \mu\text{m}$. This laser had a tuning bandwidth in excess of 220 nm with output power of 25 mW and side-mode suppression ratio up to 55 dB, indicating emission in highly single-mode regime.

Mode-hopping characteristics of this laser is shown in Fig. 11 and Fig. 12. As per Fig. 11, the mirror is rotated in steps of 0.01° , yielding mode hops of 17.7 GHz per step, fully controlled by the mirror tilt angle. For comparison the Free Spectral Range (FSR) of the free-running chip is 40 GHz and the FSR of the ECDL cavity is 1.7 GHz. Their impact is not

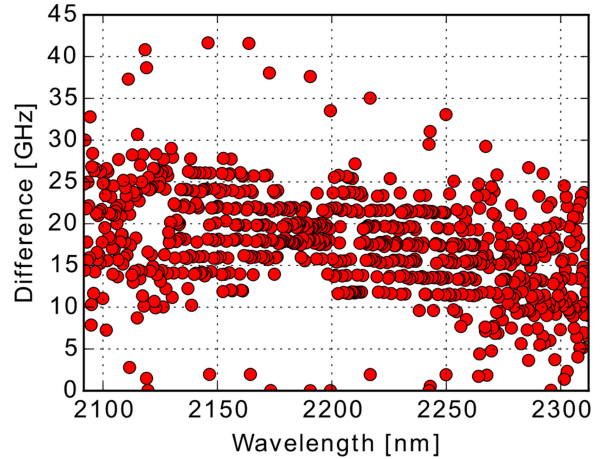


Fig. 12. Wavelength change at each tuning step.

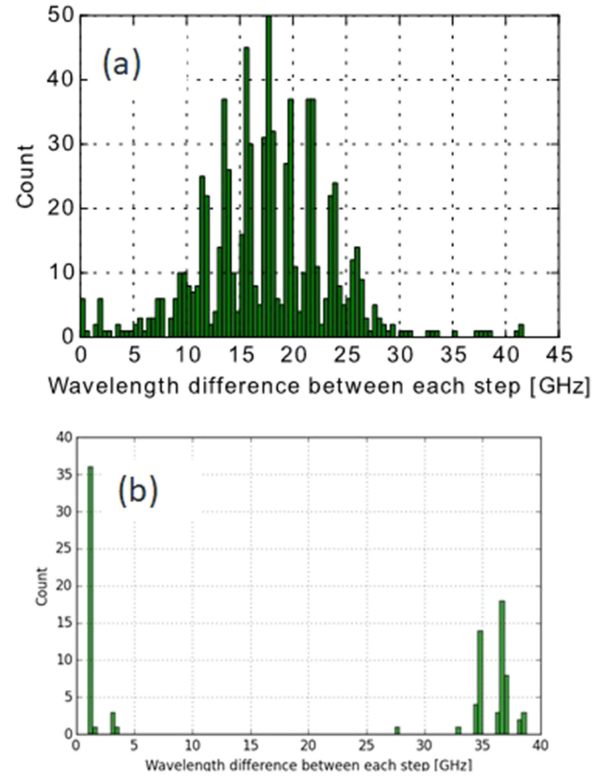


Fig. 13 Wavelength hopping histograms for two SWLs.

seen in distribution of the frequency change at each tuning step (Fig 12), although they can be appreciated by plotting a histogram of the frequency step distribution.

In Fig. 13a, the 1.7 GHz steps at external cavity FSR are clearly visible, affirming the spectral purity of the ECDL and an excellent AR coating. A case, where the AR coating reflectivity was not as good is shown in Fig. 13. Here, while the nominal facet reflectivity was supposed to be similar as for the gain-chip in Figs. 10–12, the mode hops at the external cavity FSR are distributed non-uniformly and the chip FSR dominates in the tuning curve despite that the SMSR for this laser is still high, of 43 dB.

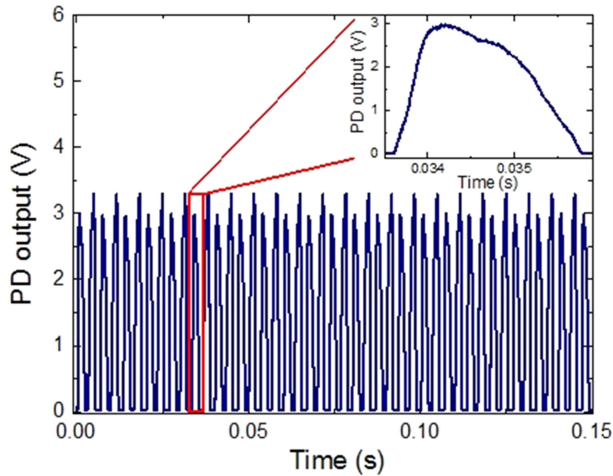


Fig. 14. SWL sweep train, when the MEMS mirror is driven at 150 Hz. The inset shows a zoom-in into a single gain-bandwidth sweep of the gain-chip.

TABLE II
PERFORMANCE SUMMARY FOR GaSb SWEPT-WAVELENGTH LASERS*

λ_{center} (nm)	P_{max} (mW)	BW @ ≥ 10 mW (cm^{-1})
1730	16	168
1920	50	380
2100	48	627
2250	35	595
2300	38	471
2380	30	300

* λ_{center} – is the center wavelength of the gain curve, P_{max} – is the maximum output power within the tuning curve, BW @ ≥ 10 mW – is the tuning bandwidth while maintaining 10 mW or higher output power.

Another important aspect of the MEMS tunable GaSb SWL is the wavelength tuning speed. As mentioned in the earlier paragraph, the MEMS mirror used in the SWL has a mechanical resonant frequency of ~ 200 Hz, which limits the maximum tuning speed. Experimentally, we have observed that 150 Hz MEMS drive frequency is the upper useful limit for our SWLs. In practice, the wavelength sweep is performed twice per cycle – i.e., the MEMS mirror moves forwards and then backwards. This allows us to collect 300 spectral scans per second. Fig. 14 illustrates a train of SWL sweeps recorded with a fast photodiode during 150 ms interval, when the MEMS mirror is driven at 150 Hz. From Table II and Figs. 8 and 9, it can be seen that for most of the gain-chips the wavelength tuning speed is $60'000 \text{ cm}^{-1}/\text{s}$ (considering the average bandwidth of 400 cm^{-1}), and can reach up to $188'100 \text{ cm}^{-1}/\text{s}$ for SWL with a gain-chip bandwidth of $\sim 627 \text{ cm}^{-1}$. To the best of our knowledge, these tuning speeds are not only beyond the state-of-art ECDLs but also when compared to the tunable solid-state OPO-based lasers.

E. Frequency Noise and Linewidth

For the linewidth measurement in GaSb SWLs, we used Si wafer as a frequency discriminator. The Si wafer was uncoated and of 1.5 mm thick, and was used as a Fabry-Perot (FP) etalon with a fineness of 2.5 and free spectral range of 28.5 GHz. By tilting the incident angle within $\pm 2^\circ$ off the axis, we

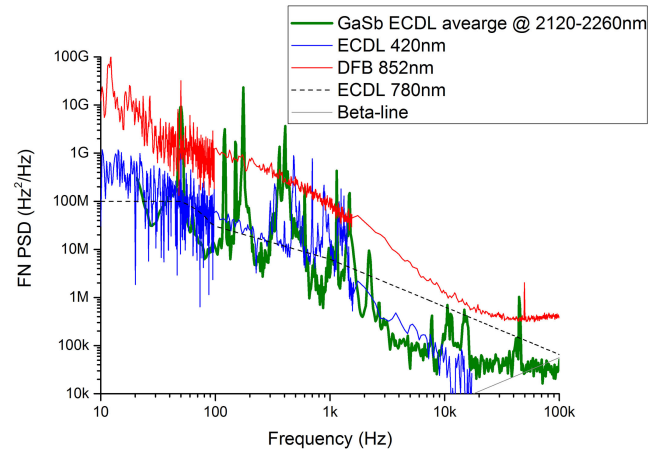


Fig. 15. Power spectral density of frequency noise in GaSb ECDL, averaged over the spectral tuning range. For comparison, FN PSD in 852 nm DFB and 420 nm and 780 nm ECDLs are shown (based on data from [25] and [26]).

tuned the FP fringe on and off the resonance with the laser emission frequency. The frequency noise (FN) measurement were performed by tilting the FP etalon angle to the half of the transmission fringe, where the AM-FM conversion slope has a maximum. The measured slope of our discriminator was 90 1/THz^{-1} for the conversion of the FM noise into relative intensity noise (RIN). The transmitted optical signal was fed to a TEC-cooled InGaAs p-i-n photodetector (Hamamatsu G5853-203) followed by a variable-gain trans-impedance amplifier (Femto, DHPA-100) and monitored on an FFT spectrum analyzer (Agilent HP89410A). The intensity noise was first measured with the Si etalon tilted for a transmission maximum and then tilted for the half of the transmission fringe in order to superimpose the converted frequency noise onto the laser relative intensity noise. At the end, the FN PSD is extracted by taking the RIN difference and scaling it with the discriminator slope.

The measurements were performed for several emission wavelengths across the entire spectral tuning range in our GaSb SWL. Within the noise limit of our setup and the acoustic noise sensitivity of the MEMS mirror, we have not noticed a significant effect of the wavelength tuning on the measured FN power spectra density (PSD). Fig 15 shows the FN PSD averaged between the curves taken at different wavelengths.

As expected, FN in our ECDL are smaller than that of a DFB laser. Unfortunately no literature data on FN PSD in GaSb DFB lasers is known to the authors so as the comparison is made with a GaAs DFB device laser used in atomic spectroscopy at 852 nm [25]. Figure 15 also provides a comparison with two other ECDLs. Apparently, all ECDLs in virtue of longer cavities have smaller linewidths than DFB. One of the two selected reference external cavity lasers was a free-running GaN based ECDL operating at 420 nm wavelength [25] and another one was a GaAs based actively stabilized ECDL at 780 nm [26]. Note that in contrast to our Littman-Metcalf GaSb ECDL, all cited ECDLs utilize Littrow cavity configuration.

The lasing linewidths in these lasers are estimated from the measured FN spectra utilizing the method from [27]. In Fig 16,

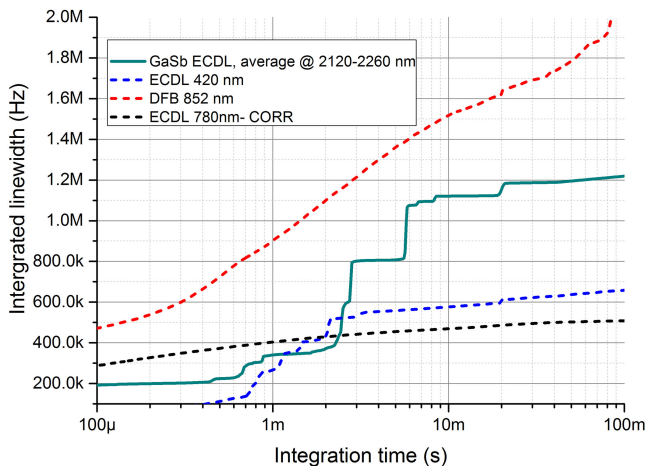


Fig. 16. Estimated linewidth of GaSb ECDL vs integration time. The linewidth averaged over the spectral wavelength tuning range is shown. For comparison, integrated linewidth of 852 nm DFB and 420 nm ECDL are shown based on the data from [25] and [26].

the linewidth is plotted as function of the integration time set by the duration of the linewidth measurement experiment.

More specifically, the lasing linewidth FWHM is equal to $(8 \cdot \ln 2)^{1/2}$ multiplied by the square root of the FN integrated from the cut-off frequency corresponding to the inverse of the integration time up to the intercept of the frequency-noise curve and the line $8f \cdot \ln 2 / \pi^2$ labeled “beta-line” in Fig. 15.

Despite the different gain materials and wavelengths, for the integration times of ~ 1 ms, all ECDLs show comparable performance in terms of linewidth, which is in the 300 kHz–400 kHz range. Note that this integration time corresponds to FN contribution from the Fourier frequency range 1 kHz to ~ 20 –50 kHz with the FN curve slope $\sim 1/f$ dominated by the flicker noise. At low Fourier frequencies, FN curve in our GaSb MEMS based ECDL reveals several acoustic bumps which extend from 100 Hz to 2 kHz, and have higher spectral amplitudes than in 420 nm ECDL. Respectively the linewidth vs integration time curve shows a clear step each time a new acoustic resonance enters the bandwidth of the linewidth integration setup. The enhanced acoustic sensitivity may be attributed to the use of MEMS mirror with the lightweight flexure mechanism as compared to the rigid volumetric metal mounts used in other ECDLs. Note that strong acoustic sensitivity does not allow us to conclude on the spectral dependence of FN across the wavelength tuning range in our GaSb ECDL. As a result, the linewidth for integration times > 2 ms in MEMS based GaSb ECDL exceeds the linewidths of other ECDLs in Fig. 16. Yet at any integration time it remains well below the linewidth of the quoted DFB laser for atomic spectroscopy applications and it is well sufficient for a majority of spectroscopy applications. For example, Doppler linewidth broadening of an Rb atomic transition at room temperature is much larger, of ~ 600 MHz. The acoustic contribution to the FN noise is expected to be suppressed in ECDL configuration without mechanically moving parts such as GaSb gain-chip integrated with Si photonic integrated circuit [19], [18].

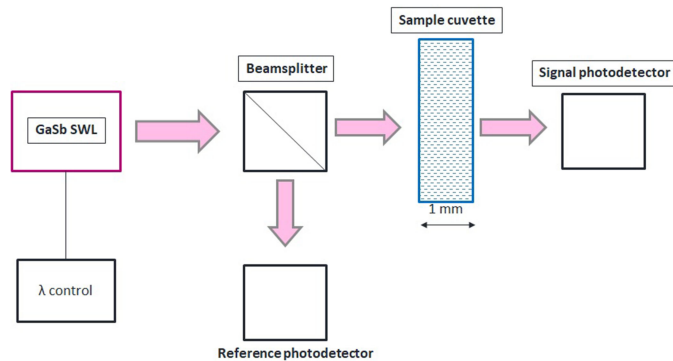


Fig. 17. Schematic block diagram of three SWL-based spectroscopic sensor for critical biomolecules [17].

IV. SPECTROSCOPIC BIOSENSING WITH GaSb SWEPT-WAVELENGTH LASERS

A. Spectroscopic Sensor Concept

The use of swept-wavelength laser allows a spectroscopic sensor to be realized in a straight-forward way. In the simplest case, it comprises only the SWL and a photodetector. In practical realization, some additional functions such as wavelength control and calibration have to be added. Fig. 17 depicts a schematic block diagram of an array of three SWLs used for spectroscopic sensing of some of the main biomolecules [17].

Here, the output beams of one or more GaSb SWLs are collimated and combined into a single beam which is sent through a cuvette with the physiological substance. The signal is collected with a single TEC-stabilized extended GaInAs photodetector. An additional wavelength control and calibration module (not shown in the figure) is deployed to account for the nonlinearities due to MEMS mirror tuning as well as to provide an absolute wavelength calibration.

B. Biosensing Applications

As a proof-of-concept of the spectroscopic sensing of multiple molecules using GaSb SWL, we target different bio-molecules: glucose, lactate, urea and bovine serum albumin. Each of the molecules act as relevant biomarkers and/or important baseline contributors that need to be taken into account when performing remote sensing experiment.

Fig. 18 shows experimental absorbance spectrum of a bovine serum albumin (BSA) in tris-buffer saline solution, which was used to simulate human serum albumin (HSA) – the most dominant protein in human blood plasma and thus a very important and strong baseline contributor. In this picture three GaSb SWLs were used to record the entire BSA specific spectrum, spanning across more than 500 nm. The result clearly illustrates the effect of strong collisional broadening of the absorption spectra and the necessity of ultra-broad tunable lasers.

Blood glucose, lactate and urea represent one of the most important biomolecules that can act as indicators or markers for important physiological processes. In particular, this addresses chronic diseases such as type-I and type-II diabetes, where glucose is the dominant key marker, however in advanced stages

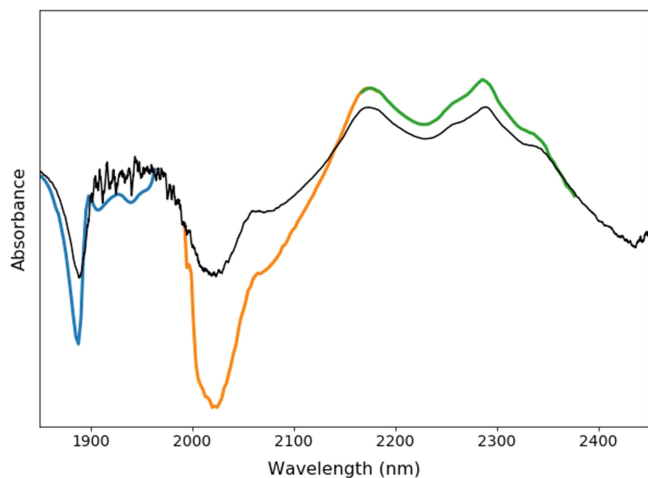


Fig. 18. Absorbance spectrum of bovine serum albumin recorded with a three-SWL based spectroscopic sensor. Each laser is indicated by the different color. The black line represents measurements with a commercial table-top FTIR instrument. Reproduced from [17].

of diabetes it might be critical to monitor lactate and urea at the same time as they could provide early indication of serious complications such as ketoacidosis and lactic acidosis [28]. Aside from diabetes, lactate is an important clinical marker and mortality indicator for severe sepsis cases [29]. In addition to clinical relevance, glucose and lactate are key metabolites for athlete performance monitoring as they provide insight into metabolism and muscle performance [30]. All of the mentioned applications represent extremely important and large markets with potential effect for not only cost-saving for the healthcare system but also improving the quality of life and in some cases life-saving. According to World Health Organization (WHO), in 2014, diabetes alone affected lives of more than 400 million people worldwide. Therefore, the market potential for laser-based spectroscopic sensor technology is extremely large. We have demonstrated the possibility to use GaSb SWL technology to measure lactate, urea, serum albumin and glucose earlier [17], thus in this paper we focus on the possibility to not only demonstrate proof-of-concept possibility for sensing these important bio-molecules but also to quantitatively assess the potential of such GaSb-SWL based sensor. The next section describes the implementation our GaSb SWL based sensor for calibrated remote sensing of blood glucose. For this purpose, a single, broadband SWL with tuning bandwidth of $\sim 500 \text{ cm}^{-1}$ was implemented in the sensor architecture.

C. GaSb Swept-Wavelength Laser-Based Glucose Sensor

Biosensing must provide an accurate prediction of the concentration level of the target molecule. Therefore we performed a large number of measurements of different glucose concentrations in order to construct concentration calibration model based on the multivariate partial least square (PLS) based algorithm [31], [32]. Using GaSb-based SWL based on a gain-chip with extremely wide tuning bandwidth (Fig. 9) as a light source has a great advantage since it provides access to an extremely large number of molecule specific wavelengths that can

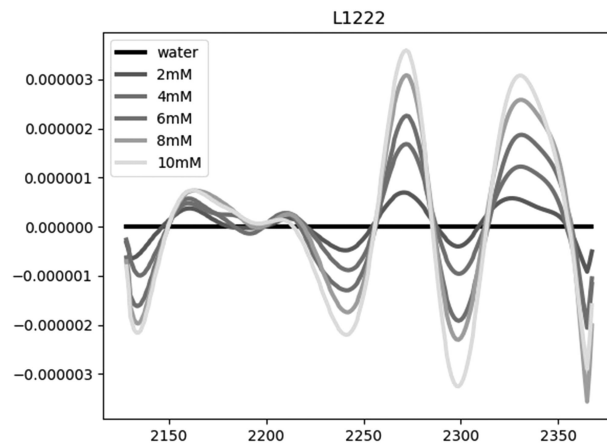


Fig. 19. Second-order derivative of transmittance spectra for different glucose concentrations obtained with GaSb-based SWL.

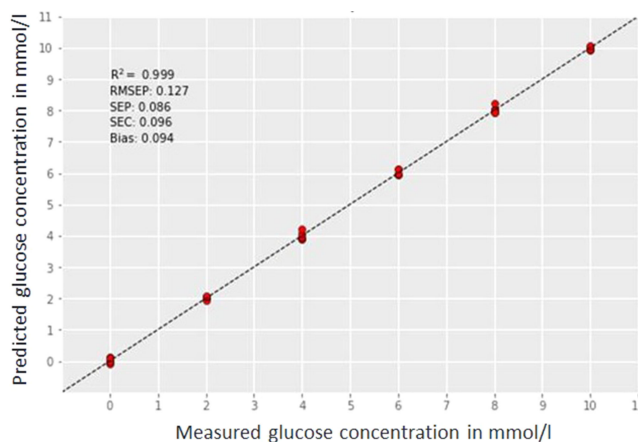


Fig. 20. Experimental sensor calibration curve for synthetic glucose solution in TBS matrix.

be used to construct the prediction algorithm. For example, in our case, the concentration calibration algorithm for glucose in TBS solution was constructed by selecting around 100 wavelengths that are most significant to prediction. Fig. 19 shows second-order derivative of experimental glucose transmittance spectra, whereas Fig. 20 illustrates the experimental sensor glucose concentration calibration curve.

To obtain the sensor calibration curve in Fig. 20, we measured 150 datasets of TBS solution with different glucose concentration in the 2–10 mmol/l range. Around 120 of the datasets were used to create the calibration model and 30 randomly selected datasets were used for prediction validation. The results yielded excellent sensor performance with determination coefficient of 99.9% and a root-mean-square-error-of-prediction (RMSEP) of 0.13 mmol/l.

In practical cases, measurement of glucose concentration level is more challenging as it has to be measured from whole blood, which, by nature, is a very complex physiological substance with a large number of different constituents such as forming elements, different proteins, and other molecules.

To validate our GaSb-based SWL spectroscopic sensor, 28 volunteers, following the signature of the Informed Consent Form, were subjected to glucose tolerance test. The test was

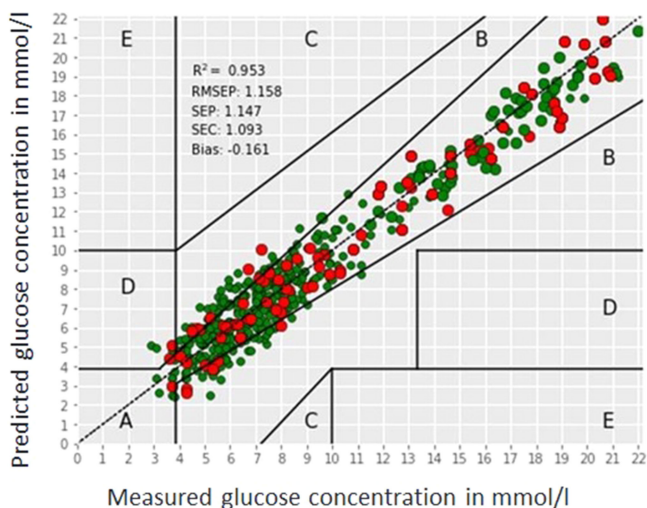


Fig. 21. Experimental sensor calibration curve in case of glucose in whole blood in mmol/l. Here, the green dots represent datasets used to build the calibration model, and red dots indicate the data sets used for validation.

TABLE III
GLUCOSE SENSOR PERFORMANCE IN WHOLE BLOOD

Parameter	Value
No. of datasets	>500
R^2	95.3 %
Concentration range	3–20 mmol/l
RMSEP	1.15 mmol/l
No. of points in A zone	85%
MARD	10.8%

R^2 – determination coefficient, RMSEP- Root Mean Square Error of Prediction, MARD- Mean Absolute Relative Difference

performed by means of oral intake of solution containing 75 g of glucose. The series of venous blood sampling were performed repeatedly during the course of approximately 2 hours. The group of volunteers contained healthy individuals as well as type-I and type-II diabetics. In order to build a library of whole blood data for the calibration algorithm, we used a commercial clinical blood analyzer (Piccolo from Abaxis), used as a gold standard. We then used the calibration model to predict glucose concentration from the spectroscopic measurements obtained with GaSb based SWL sensor. In total over 500 datasets were obtained from 28 different individuals during the course of approximately 1 month. Fig. 21 shows the experimental calibration curve of the SWL-based spectroscopic sensor in case of glucose sensing in whole blood. The sensor performance is summarized in Table III.

Experimental data demonstrate the excellent glucose concentration prediction performance even in such complex matrix as whole blood. As per Table III, determination coefficient of 95% in combination with 1.15 mmol/l RMSEP and MARD values of 10.8% is achieved. This marks significant sensitivity improvement compared to prior art [33], [34], which mainly focus on synthetic solutions. In addition these results already compare well with clinical device requirements [35] and requirements as per ISO 15197:2015 standard.

V. CONCLUSION

In this paper we presented comprehensive results on the GaSb-based swept-wavelength laser technology for 1.7–2.5 μm spectral region. A large part of the presented results go beyond-state-of-the-art for the discussed field of technology such as ultra-broad wavelength tuning of 627 cm^{-1} per single chip with output power in excess of 20 mW and wavelength tuning speed of 188 000 cm^{-1}/s . In addition, we provided useful insight into microscopic parameters of GaSb type-I QW based gain-chips as well as external cavity linewidth and noise performance. Furthermore, we demonstrated a real-life application example of a GaSb SWL-based spectroscopic sensor for critical biomolecules, including excellent sensor performance in case of glucose sensing in whole blood. Demonstrated experimental results are already very close to the requirements of ISO 15197:2015.

REFERENCES

- [1] M. W. Sigrist, "Mid-infrared laser-spectroscopic sensing of chemical species," *J. Adv. Res.*, vol. 6, no. 3, pp. 529–533, 2015.
- [2] J. A. Gupta, P. J. Barrios, J. Lapointe, G. C. Aers, and C. Storey, "Single-mode 2.4 μm InGaAsSb/AlGaAsSb distributed feedback lasers for gas sensing," *Appl. Phys. Lett.*, vol. 95, no. 4, pp. 111–114, 2009.
- [3] G. A. Mark, "Diode laser absorption sensors for gas-dynamic and combustion flows," *Meas. Sci. Technol.*, vol. 9, no. 4, pp. 545–562, 1998.
- [4] A. Schwaighofer, M. R. Alcaráz, C. Araman, H. Goicoechea, and B. Lendl, "External cavity-quantum cascade laser infrared spectroscopy for secondary structure analysis of proteins at low concentrations," *Sci. Rep.*, vol. 6, pp. 1–10, 2016.
- [5] C. Young *et al.*, "External cavity widely tunable quantum cascade laser based hollow waveguide gas sensors for multianalyte detection," *Sens. Actuators B, Chem.*, vol. 140, pp. 24–28, 2009.
- [6] B. G. Lee *et al.*, "Widely tunable single-mode quantum cascade laser source for mid-infrared spectroscopy," *Appl. Phys. Lett.*, vol. 91, no. 23, pp. 89–92, 2007.
- [7] L. A. Coldren, "Monolithic tunable diode lasers," *IEEE J. Sel. Topics Quantum Electron.*, vol. 6, no. 6, pp. 988–999, Nov./Dec. 2000.
- [8] R. Todt *et al.*, "Sampled grating tunable twin-guide laser diodes with over 40-nm electronic tuning range," *IEEE Photon. Technol. Lett.*, vol. 17, no. 12, pp. 2514–2516, Dec. 2005.
- [9] G. Wysocki *et al.*, "Widely tunable mode-hop free external cavity quantum cascade lasers for high resolution spectroscopy and chemical sensing," *Appl. Phys. B Lasers Opt.*, vol. 92, pp. 305–311, 2008.
- [10] A. Q. Liu and X. M. Zhang, "A review of MEMS external-cavity tunable lasers," *J. Micromechanics Microengineering*, vol. 17, no. 1, pp. R1–R13, 2007.
- [11] A. K. Amerov, J. Chen, and M. A. Arnold, "Molar absorptivities of glucose and other biological molecules in aqueous solutions over the first overtone and combination regions of the near-infrared spectrum," *Appl. Spectrosc.*, vol. 58, no. 10, pp. 1195–1204, 2004.
- [12] M. Rattunde *et al.*, "Emitting in the 1.9 To 2.4 Mm Wavelength Range," vol. 2931, no. 1997, p. 79108, 2004.
- [13] E. Geerlings *et al.*, "Widely tunable GaSb-based external cavity diode laser emitting around 2.3 μm ," *IEEE Photon. Technol. Lett.*, vol. 18, no. 18, pp. 1913–1915, Oct. 2006.
- [14] K. Vizbaras and M. C. Amann, "Room-temperature 3.73 μm GaSb-based type-I quantum-well lasers with quaternary barriers," *Semicond. Sci. Technol.*, vol. 27, no. 3, 2012, Art. no. 032001.
- [15] K. Vizbaras and M.-C. Amann, "3.6 μm GaSb-based type-I lasers with quaternary barriers, operating at room temperature," *Electron. Lett.*, vol. 47, no. 17, 2011, Art. no. 980981.
- [16] K. Vizbaras *et al.*, "High power continuous-wave GaSb-based superluminescent diodes as gain chips for widely tunable laser spectroscopy in the 1.95–2.45 μm wavelength range," *Appl. Phys. Lett.*, vol. 107, no. 1, 2015, Art. no. 011103.

- [17] A. Vizbaras *et al.*, “Swept-wavelength lasers based on GaSb gain-chip technology for non-invasive biomedical sensing applications in the 1.7–2.5 μm wavelength range,” *Biomed. Opt. Express*, vol. 9, no. 10, pp. 4834–4849, 2018.
- [18] R. Wang *et al.*, “Compact GaSb/silicon-on-insulator 2.0x μm widely tunable external cavity lasers,” *Opt. Express*, vol. 24, no. 25, pp. 28977–28986, 2016.
- [19] R. Wang *et al.*, “III–V-on-silicon photonic integrated circuits for spectroscopic sensing in the 2–4 μm wavelength range,” *Sensors*, vol. 17, no. 8, 2017, Art. no. 1788.
- [20] C. H. Henry, “Theory of the linewidth of semiconductor lasers,” *IEEE J. Quantum Electron.*, vol. 18, no. 2, pp. 259–264, Feb. 1982.
- [21] G. E. Shtengel, R. F. Kazarinov, G. L. Belenky, M. S. Hybertsen, and D. A. Ackerman, “Advances in measurements of physical parameters of semiconductor lasers,” *Int. J. High Speed Electron. Syst.*, vol. 9, no. 4, pp. 901–940, 1998.
- [22] T. Feng, L. Shterengas, T. Hosoda, A. Belyanin, and G. Kipshidze, “Passive mode-locking of 3.25 μm GaSb-based cascade diode lasers,” *ACS Photon.*, vol. 5, pp. 4978–4985, 2018.
- [23] M. Wang *et al.*, “External cavity type-I quantum well cascade diode lasers with a tuning range of 440 nm near 3 μm ,” *Opt. Lett.*, vol. 43, no. 18, pp. 4473–4476, 2018.
- [24] J. M. Breguet *et al.*, “Tunable extended-cavity diode laser based on a novel flexure-mechanism,” *Int. J. Optomechatronics*, vol. 7, no. 3, pp. 181–192, 2013.
- [25] X. Zeng and D. L. Bořko, “1/f noise in external-cavity InGaN diode laser at 420 nm wavelength for atomic spectroscopy,” *Opt. Lett.*, vol. 39, no. 6, pp. 1685–1688, 2014.
- [26] L. D. Turner, K. P. Weber, C. J. Hawthorn, and R. E. Scholten, “Frequency noise characterisation of narrow linewidth diode lasers,” *Opt. Commun.*, vol. 201, no. 4–6, pp. 391–397, 2002.
- [27] P. T. Gianni Di Domenico and S. Schilt, “Simple approach to the relation between laser frequency noise and laser line shape,” *Appl. Opt.*, vol. 49, no. 25, pp. 4801–4807, 2010.
- [28] P. English and G. Williams, “Hyperglycaemic crises and lactic acidosis in diabetes mellitus,” *Postgraduate Med. J.*, vol. 80, no. 943, pp. 253–261, 2004.
- [29] M. E. Mikkelsen *et al.*, “Serum lactate is associated with mortality in severe sepsis independent of organ failure and shock,” *Crit. Care Med.*, vol. 37, no. 5, pp. 1670–1677, 2009.
- [30] B. F. Miller *et al.*, “Lactate and glucose interactions during rest and exercise in men: Effect of exogenous lactate infusion,” *J. Physiol.*, vol. 544, no. 3, pp. 963–975, 2002.
- [31] M. A. Arnold, L. Liu, and J. T. Olesberg, “Selectivity assessment of noninvasive glucose measurements based on analysis of multivariate calibration vectors,” *J. Diabetes Sci. Technol.*, vol. 1, no. 4, pp. 454–462, 2007.
- [32] J. T. Olesberg, L. Liu, V. Van Zee, and M. A. Arnold, “In vivo near-infrared spectroscopy of rat skin tissue with varying blood glucose levels,” *Analytical Chem.*, vol. 78, no. 1, pp. 215–223, 2006.
- [33] J. T. Olesberg, M. A. Arnold, C. Mermelstein, J. Schmitz, and J. Wagner, “Tunable laser diode system for noninvasive blood glucose measurements,” *Appl. Spectrosc.*, vol. 59, no. 12, pp. 1480–1484, 2005.
- [34] E. Ryckeboer, R. Bockstaele, M. Vanslembrouck, and R. Baets, “Glucose sensing by waveguide-based absorption spectroscopy on a silicon chip,” *Biomed. Opt. Express*, vol. 5, no. 5, pp. 1636–1648, 2014.
- [35] T. S. Bailey, “Clinical implications of accuracy measurements of continuous glucose sensors,” *Diabetes Technol. Therapeutics*, vol. 19, no. S2, pp. S-51–S-54, 2017.



Augustinas Vizbaras received the B.S. degree in electrical engineering from Vilnius University, Vilnius, Lithuania, in 2007 and the M.Sc. degree in physics from Royal Institute of Technology, Stockholm, Sweden, in 2009. He was a doctoral candidate in the field of semiconductor technology with Walter Schottky Institut, TU Munich, Germany, in 2009–2012. In 2011, he cofounded Brolis Semiconductors, where he currently heads the chip technology and sensor activities. He has authored or coauthored more than 50 papers in scientific peer-reviewed journals

and conference proceedings, three granted U.S. patents, and nine pending international patent applications. He was awarded with Order of Merit to Lithuania Knights Cross in 2017, Medal for Distinguished Service from Lithuanian Special Operation Forces in 2018, and Medal for Merit to Lithuania's Riflemen's Union in 2015.



Ieva Šimonytė received the M.Sc. degree in material science and semiconductors physics from Vilnius University, Vilnius, Lithuania, in 2014. Since 2013, she has been working as Computational Simulation Engineer with Brolis Semiconductors, Vilnius, Lithuania. Her activities include electrical, thermal and optical modeling of semiconductor material, devices and systems, simulations of light interaction with living body and statistical data analysis. She has authored or coauthored more than 15 papers in scientific peer-reviewed journals and conference proceedings and six pending patent applications.



Serge Droz received the Mechanical Engineer degree from HES, Le Locle, Switzerland. Since 1991, he has been an R&D Engineer with CSEM SA, Neuchâtel, Switzerland, involved in various development and production of instrumentation for surface characterization. In 1997, he joined the Mechanism Section for advanced projects for space and astronomy applications, was also involved as a Project Manager of industrial mechatronics projects in the watch and medical domains.



Nicolas Torcheboeuf received the M.Sc. degree in applied physics from EPFL, Lausanne, Switzerland, in 2016. During his master's thesis, he did research on the stabilization of diode pumped solid-state lasers. Since 2016, he has been working as an R&D Engineer with the Systems Division, CSEM SA, Neuchâtel, Switzerland. His activities are mainly focused on the development of ultra-fast lasers, tunable external-cavity diode lasers, and high power chirped-pulse amplifier systems.



Arūnas Miasojedovas received the B.Sc. degree in applied physics in 2007, the M.Sc. degree in materials science and semiconductors physics in 2009, and the Ph.D. degree in 2013, working on the topic “Control of fluorescence properties of organic optoelectronic materials by molecular aggregate formation,” from Vilnius University, Vilnius, Lithuania. Later, he spent two years as a Postdoctoral in an Organic Electroactive Materials research group, led by Prof. A. Monkman at Durham University, where he studied triplet harvesting processes and produced OLED devices.

In 2017, he joined Brolis Semiconductors team and, since then, has been involved in the development of spectroscopic laser sensor technology.



Augustinas Trinkūnas received the B.Sc. and M.Sc. degrees in electrical engineering from Vilnius University, Vilnius, Lithuania, in 2012 and 2014, respectively. Since 2013, he has been an Epitaxy Engineer with Brolis Semiconductors, Vilnius, Lithuania. His activities are mainly focused the molecular beam epitaxial growth of GaSb-based optoelectronic devices. He has coauthored more than 15 publications in peer-reviewed journals and conference proceedings.



Antanas Gulbinas received the Ph.D. degree in 2003 from Kaunas University of Medicine, Kaunas, Lithuania, followed by license of Abdominal Surgery in 2004. He is currently the Head of the Laboratory of Surgical Gastroenterology, Institute for Digestive Research, Lithuanian University of Health Sciences, Kaunas, Lithuania. He is experienced in molecular biology research (methods of proteomics and genomics) with an experience of four clinical trials. He has a perfect knowledge of methodology of scientific research, biostatistics, statistical computational methods and coauthored two books on the research methodology. From 2013 to 2016, he was a Council Member of the European Digestive Surgery Society (EDS), for the Training and Education. Since 2013, he has been Yearly Faculty Member of postgraduate courses with EDS. Since 2014, he has been a Member of the Board of Nordic Pancreas Forum of Excellence, Chronic Pancreatitis Initiative. Since 2017, he has been a Member of the Research Board of United European Gastroenterology (UEG).



Tadas Bučiūnas received the M.Sc. degree in physics from Vilnius University, Vilnius, Lithuania, in 2018. He did his master's thesis project as Intern at Brolis Semiconductors, where since 2018, he has been a Full-Time R&D Engineer in the field of spectroscopic sensor technology.



Dmitri L. Boiko received the Diploma (with Hons.) in applied mathematics and physics, the M.Sc. degree (with Hons.) in laser physics from the Moscow Institute of Physics and Technology, Dolgoprudny, Russia, in 1993, and the Ph.D. degree from the Moscow Institute of Physics and Technology and Research & Development Institute "Polyus," Moscow, Russia. He has been working on dynamics of solid state ring lasers, multisection semiconductor edge emitting lasers, quantum cascade lasers, vertical cavity surface emitting lasers as well as phase coupled laser arrays. His career path propagates via Ecole Nationale Supérieure de Sciences Appliquées et de Technologie in Lannion (ENSSAT) in France, and Ecole Polytechnique Fédérale de Lausanne (EPFL) in Switzerland. Since 2008, he has been with the Center Suisse d'Electronique et de Microtechnique in Neuchatel, as a Senior Expert. His current research activities are focused on the atomic clocks and gyroscopes as well as ultrafast lasers.



Žilvinas Dambrauskas received the Ph.D. degree, working on the topic "Inhibition of Heme Oxygenase-1 (HO-1) increases responsiveness of pancreatic cancer cells to anticancer treatment," from Heidelberg Ruprecht-Karls-Universität, Heidelberg, Germany, under supervision of Prof. H. Friess in 2005. He is currently the Head of the LSMU CEBM, Kaunas, Lithuania. He was a Professor and an Abdominal Surgeon with the Department of Surgery, LSMU. He has been on a number of clinical rotations and placement since at the best-known clinics

in the U.K., USA, France, Germany, Sweden, and Belgium and has coauthored more than 50 scientific papers and several textbooks. But he proudly admits that the whole journey started with the studies at the Secondary and high school No. 5, Panevezys, Lithuania, and a year at Ashville College, Harrogate, England, after winning a scholarship established by the G. Soros Foundation and the Open Society Fund-Lithuania.



Kristijonas Vizbaras received the B.S. degree in electrical engineering from Vilnius University, Vilnius, Lithuania, in 2007 and the M.Sc. degree in physics from Royal Institute of Technology, Stockholm, Sweden, in 2009. He was a doctoral candidate in the field of semiconductor technology with Walter Schottky Institute, TU Munich, Germany, in 2009–2012. In 2011, he cofounded Brolis Semiconductors, where he currently heads the epitaxial growth activities. He has authored or coauthored more than 50 papers in scientific peer-reviewed journals and conference proceedings, two granted US patents, and nine pending patent applications. He was awarded with Order of Merit to Lithuania Knights Cross in 2017, Medal for Distinguished Service from Lithuanian Special Operation Forces in 2018, and Medal for Merit of Lithuania's Riflemen's Union in 2015.